Journal of Quantitative Spectroscopy & Radiative Transfer 133 (2014) 538–550

Contents lists available at ScienceDirect

Journal of Quantitative Spectroscopy & Radiative Transfer

journal homepage: www.elsevier.com/locate/jqsrt

Effects of ozone and relative humidity on fluorescence spectra of octapeptide bioaerosol particles

Yong-Le Pan [a,*], Joshua L. Santarpia [b], Shanna Ratnesar-Shumate [c], Elizabeth Corson [c], Jonathan Eshbaugh [c], Steven C. Hill [a], Chatt C. Williamson [a], Mark Coleman [a], Christopher Bare [c], Sean Kinahan [c]

[a] US Army Research Laboratory, Adelphi, MD 20783, USA
[b] Sandia National Laboratories, Albuquerque, NM 87123, USA
[c] Johns Hopkins University Applied Physics Laboratory, Laurel, MD 20723, USA

ARTICLE INFO

Article history:
Received 23 July 2013
Received in revised form
16 September 2013
Accepted 17 September 2013
Available online 27 September 2013

Keywords:
Octapeptide bioerosol particles
Fluorescence spectra
Atmospheric age and process
Ozone oxidation
Relative humidity
Rotating reaction chamber

ABSTRACT

The effects of ozone and relative humidity (RH) at common atmospheric levels on the properties of single octapeptide bioaerosol particles were studied using an improved rotating reaction chamber, an aerosol generator, an ultraviolet aerodynamic particle sizer (UVAPS), an improved single particle fluorescence spectrometer (SPFS), and equipments to generate, monitor and control the ozone and RH. Aerosol particles (mean diameter ~2 μm) were generated from a slurry of octapeptide in phosphate buffered saline, injected into the rotating chamber, and kept airborne for hours. Bioaerosols were sampled from the chamber hourly for the measurements of particle-size distribution, concentration, total fluorescence excited at 355-nm, and single particle fluorescence spectra excited at 266-nm and 351-nm under different controlled RH (20%, 50%, or 80%) and ozone concentration (0 or 150 ppb). The results show that: (1) Particle size, concentration, and the 263-nm-excited fluorescence intensity decrease at different rates under different combinations of the RH and ozone concentrations used. (2) The 263-nm-excited UV fluorescence (280–400 nm) decreased more rapidly than the 263-nm-excited visible fluorescence (400–560 nm), and decreased most rapidly when ozone is present and RH is high. (3) The UV fluorescence peak near 340 nm slightly shifts to the shorter wavelength (blue-shift), consistent with a more rapid oxidation of tryptophan than tyrosine. (4) The 351/355-nm-excited fluorescence (430–580 nm/380–700 nm) increases when ozone is present, especially when the RH is high. (5) The 351/355-nm-excited fluorescence increase that occurs as the tryptophan emission in the UV decreases, and the observation that these changes occur more rapidly at higher RH with the present of ozone, are consistent with the oxidation of tryptophan by ozone and the conversion of the resulting ozonides to N-formyl kynurenine and kynurenine.

1. Introduction

Bioaerosols, e.g., airborne bacteria, fungal spores and hyphae, pollens, algae, proteins, viruses, and fragments of the above, play important roles in public health and climate [1–3]. Various technologies have been used to study atmospheric and laboratory generated bioaerosols. They include biochemical analysis (e.g., sequencing of DNA

* Corresponding author. Tel.: +1 301 394 1381; fax: +1 301 394 4797.
E-mail address: yongle.pan.civ@mail.mil (Y.-L. Pan).

0022-4073
http://dx.doi.org/10.1016/j.jqsrt.2013.09.017

or RNA); elastic scattering; chromatography; mass, nuclear magnetic resonance (NMR), ion-mobility, fluorescence emission, break-down emission, terahertz absorption, infra-red (IR) absorption, and Raman scattering spectroscopy, [e.g., 3,4] either based on the analysis of the collection of particles or of on-line individual single particles. Although thousands of studies of bioaerosols have been published and many features of bioaerosols and their concentrations in the atmosphere have been described, and many methods and instruments for characterizing bioaerosols have been described and used, there is still more that needs to be understood about the properties and sources of these bioaerosols, and to significantly improve our ability to reliably detect and characterize bioaerosols.

Fluorescence-based bioaerosol detection and characterization systems have been developed for the early warning of possible presence of biological threat agents, for environmental monitoring, and for studies of bioaerosols and their effects on clouds, climate, etc., [e.g., 5–13]. Algorithms for using spectral measurements of, e.g., fluorescence, elastic scattering, and laser induced breakdown spectroscopy, for discriminating bioaerosols from other atmospheric aerosols rely mainly on the properties of laboratory-generated aerosols measured shortly after the aerosols were generated. Some of the studies on open-air factors (OAF) [14] are some of the exceptions to this generalization. However, the properties (including viability) or parameters obtained from laboratory measurements may change with time and with exposure to different atmospheric conditions after bioaerosols are released into the air. Therefore, it is important to study how the physical, chemical and biological properties of bioaerosols are affected by various atmospheric conditions (sunlight, temperature and gases), and to understand the fate of bioaerosols in different atmospheric environments over time. Such studies and results will expand our basic knowledge of bioaerosols, and they can lead to predictive models and algorithms for the detection of bioaerosols and aerosolized bio-threat agents in various complex atmospheric environments.

There have been many studies of atmospheric aging and processing of organic carbon aerosols and bioaerosols, particularly on the effects of ozone and simulated OAF [e.g., 14–20]. Changes in fluorescence spectra from pollens (not aerosolized) treated with ozone have been measured [19]. Some correlation between ozone and naturally occurring aerosols including fungi, pollen and other organic materials have been observed [20]. Exposure to ozone was reported to change the absorption and fluorescence of the aromatic amino acids (tryptophan (Trp), tyrosine (Tyr), and phenylalanine (Phe)) in solution and in animal tissues. N-formyl kynurinene (NFK) and kynurenine (KN) were found to be the primary products from oxidation of tryptophan [21–28]. These measurements were carried out in aqueous solutions or on samples collected from air onto substrates.

Atmospheric aging and processing of bioaerosols in the natural environment may involve many different chemical reactions which occur on different time scales (minutes, hours and days). Different sizes of bioaerosols may respond differently to various environmental conditions because of the different surface/volume ratios of the particles, which will result in different diffusion and reaction rates of the interacting gases. Continuous inspection of bioaerosols collected on a substrate, or trapped in the air, may not be adequate for understanding how bioaerosols change in the atmosphere. Particles collected on a surface may not be exposed to the same environmental conditions as they would be in the atmosphere, for several reasons: (a) the portion of the particle in contact with the collection surface may not be exposed directly to atmospheric gases as it would be in the atmosphere; (b) additional reactions may occur during to the collection process; (c)properties of particles on the surface and trapped in air may be changed from multiple times of measurements such as photo-degradation [e.g., 29], and (d) the optical properties of the particle may be affected by the surface and the angle of illumination. Therefore, a preferred way to investigate atmospheric processing of biological (or other types of) particles involves replicating or approximating atmospheric conditions for particles suspended in air, where each particle is measured only once.

This paper describes our improved laboratory system for studying changes of bioaerosols in controlled atmospheric environments. We have improved our previous apparatus in a number of ways to address issues identified in previous studies [30]. To ensure that the reaction chamber (rotating drum [30–34]) was both chemically inert and not subject to the electrostatic effects seen in previous work [30], it was constructed from stainless steel and all interior surfaces were coated with polytetrafluoroethylene (PTFE). The ozone generation was moved outside of the chamber to eliminate the possibility of radical production through water vapor photolysis. Control of the relative humidity (RH) was improved to allow a wider range of RH to be studied. As in our previous study [30], a home-built single-particle fluorescence spectrometer (SPFS) system was used to measure fluorescence spectra one-at-a-time for individual aerosol particles drawn from the drum. Capabilities to measure the elastic-scattering size for each particle, and to measure the pulse energy for each shot of the illuminating laser, were added to the SPFS so that each fluorescence spectrum could be associated with a particle size and the energy of the pulse. This allows for more useful comparisons of fluorescence intensity as the mean particles decrease in size during the whole measurement process. Also, a pulsed laser at 351 nm was added to SPFS so that fluorescence spectra could be measured with 351-nm and 263-nm excitation (not both spectra for the same particle), the 351-nm laser allows us to measure the fluorescence from the molecules within bioaerosol particles that has absorption at 351 nm but not at 263 nm. Bioaerosols were sampled from the chamber hourly for the measurements of particle size distribution, concentration, total fluorescence with 355-nm excitation, and single-particle fluorescence spectra with 266-nm and 351-nm excitation. A tryptophan-containing octapeptide subunit of thrombospondin-1 (Arg–Phe–Tyr–Val–Val–Met–Trp–Lys) was used in the experiments. This octapepetide was chosen because it contains the aromatic amino acids

but eliminates the fluorescence emission from NADH, riboflavin and other fluorophors that are present in cells and many other bioaerosols. It therefore provides a relatively clean way to study the aging of tryptophan (with tyrosine and phenylalanine) in peptides exposed to ozone with various RH. Such studies can lead to a better understanding of aging of tryptophan, peptides, and proteins, which can also help in understanding other bioaerosols. The experiments were done using different controlled RH (20%, 50%, or 80%) and ozone concentrations (0 or 150 ppb). Each experiment lasted approximately 4 h if no ozone was added and 4.5 h if ozone was added. For each combination of RH and ozone concentration the experiments were repeated three times during different days.

2. Experimental arrangements

Fig. 1 shows the overall design of the laboratory system including the aerosol generation components, RH and ozone generating, controlling and monitoring components, the rotating drum, and the aerosol measurement instruments.

2.1. Humidity control

Prior to the generation of aerosol, the drum is preconditioned to the desired RH. A reservoir hanging from the stationary axle supplies water to a piezoelectric generator, which vaporizes the water. The humidified air is then forced into the drum by pumping air through the reservoir at flow rates between 0 and 500 mL/min.

2.2. Aerosol generation

Aerosol is generated using an ultrasonic spray nozzle (Sono-Tek Corp., 06-04010), with a 30-mL syringe and pump (Sono-Tek Corp., 11-01061) set to infuse the liquid suspension at a rate of 100 μL/min. A broadband ultrasonic generator (Sono-Tek Corp., 06-05108) is used to control the nozzle frequency. It is set at 3 W. The Sono-Tek nozzle is placed at the top of an aerosol capacitance chamber (ACC)

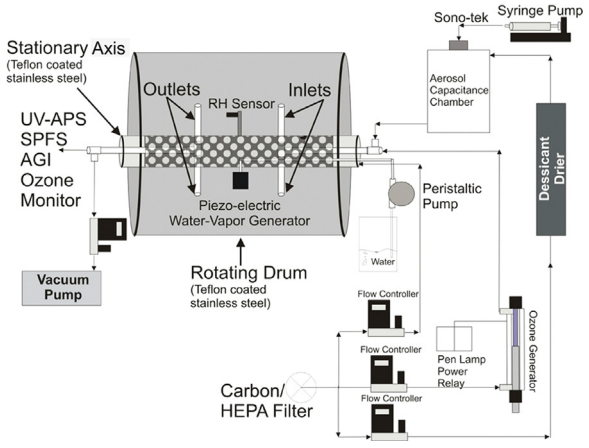

Fig. 1. Schematic of the rotating drum. The scale of the axel relative that of the drum is exaggerated to show the details of the air and aerosol flow paths, and different monitors.

that allows for mixing and initial evaporation of the droplets (initially 18 μm diameter) prior to their entering the drum. The aerosol is introduced into the drum from the ACC at a flow rate of 5 LPM.

2.3. Ozone generation

A small mercury pen lamp (Pen Ray, 97-0067-01) was placed outside the drum and shielded by a Teflon body with ports for airflow across the lamp. The mercury lamp produces deep ultraviolet light with energy sufficient to photolyze oxygen (wavelengths less than 220 nm). The singlet oxygen formed recombines with molecular oxygen (O_2) to form ozone. Dry air was sent through the lamp and into the drum at a flow rate of 50 mL/min.

2.4. Rotating drum

The rotating drum developed and used in this study consists of a ~400 L stainless steel tube capped on each end with stainless steel ends. Each end has 3 Acrylite OP4 windows, to allow penetration of UV light, for simulated solar exposure. A stainless steel perforated tube serves as the center axle of the drum. This axle is fixed, allowing the drum to rotate around it by means of a sealed bearing system attached to the end-caps of the drum. The holes in the axle allow the passage of wiring and tubing between the main drum and the inner fixed axle. All interior steel surfaces are coated with a thick layer of Teflon to prevent the steel from reacting with the gas-phase species in the drum. A Roxtec seal with 4 ports allows tubing and wiring to pass in and out of the drum. The inlet supplies the aerosol, air and water flow from the RH generator, airflow from the ozone generator, and electrical and data connections to probes inside the drum. The outlet has ports connecting tubing to the UVAPS, the SPFS, the ozone monitor, the all-glass impinger (AGI-30, Ace-Glass Inc.), and a pump for purging the air. The tubing from the fourth port is split and controlled with valves to allow separate pumps for the AGI and the system purge. Each of these pumps is connected in series after a HEPA filter and a charcoal filter to prevent any aerosol or ozone from reaching the pump and release into the laboratory.

2.5. Single-particle fluorescence spectrometer

The single-particle fluorescence spectrometer (SPFS) measurement system was developed and described previously [8,9]. The system used in this study is similar to the reported SPFS system [8] with 263 nm and 351 nm laser excitation but without the concentrator. The fluorescence spectrum detector is an Image-Intensified Charge-Coupled Device (ICCD) (Princeton Instruments, PI-Max3). Briefly, aerosol is pulled into an 18-in. cubic airtight chamber at 1 LMP from the drum, then focused into a laminar jet of around 300 μm in diameter by a sheath nozzle within the chamber. Any aerosol particles larger than 1 μm flowing through a trigger volume (~100 μm × 100 μm defined by the intersection of two diode-laser beams at 650 nm and 685 nm) will be detected by two photomultiplier tubes (PMT) and illuminated by a single pulse of 263-nm

or 351-nm laser (4th or 3rd harmonic of Nd:YLF laser, 20 μJ/pulse, ~20 ns pulse duration, 1 mm in diameter; Photonics Industries, DC-150-263 or DC-150-351). The emitted fluorescence is collected by a Schwarzschild reflective objective (Newport, numerical aperture=0.4) and dispersed by a spectrograph (Acton 150, grating 300 l/mm, blaze wavelength 500 nm). Two long-pass filters (Newport, colored-glass alternative filter) with cut wavelengths at 280 nm and 365 nm installed in a filter wheel (Princeton filter wheel FA-2448-2) mounted on the front of the spectrograph is used to block the elastic scattering of the laser at 263 nm and 351 nm respectively. Both filters have about 95% transmission 3 nm above the cut-off wavelength, and have a very steep cut-off at the indicated wavelength. Introducing the 351-nm illuminating laser into the SPFS system here allows us to further study the bioaerosols for some molecules that may have high absorption around 351 nm but with or without absorption at 263 nm.

Another two new functions are added for the measurement of particle size and pulse energy associated with each fluorescence spectrum based on the previous SPFS system [8]. A third PMT and a diode laser at 705 nm (50 mW) are used in measuring particle size. Its beam is focused about 50 μm below the trigger volume with a spatial profile about 2 mm in width and 200 μm in height. Any particles passing through the trigger volume also pass through 705-nm diode laser beam with relatively uniform intensity illumination, as its width (2 mm) is much larger compared to the trigger volume (about 100 μm). The near forward scattering (10–40°) was collected by a third PMT, amplified, and sent to a data acquisition board (Measurement Computering, MCC/USB-2523), then the digitized outputs were recorded by the computer. A photodiode was used to measure the energy of each laser pulse. The two signals from the third PMT and the photodiode are recorded only when a particle is passing through the trigger volume and a UV-LIF spectrum is measured. Therefore, the particle size, pulse energy of the illuminating UV laser (263- or 351-nm), and also the fluorescence information are recorded for each particle simultaneously. The pulse energy is less than 5% variation from pulse to pulse. The fluorescence intensity can then be normalized by the particle size and pulse energy, to correct the effects caused by particle size decreasing during the whole observing process in a few hours.

The size of each detected aerosol particle is calibrated using NIST traceable polystyrene latex (PSL) microspheres aerosolized by a Royco aerosol generator (Royco, Model 256). Calibration PSL particles are distinguished from surfactant, dust and aggregate particles, by the associated UV-LIF data from the ICCD. The particle size distribution is also confirmed by an aerodynamic particle sizer (TSI 3321) during the calibration process. Tryptophan particles, especially in the big size range (3–8 μm in diameter), are produced by an ink jet aerosol generator (IJAG, ECBC) for size calibration.

The relative spectral response for the SPFS system, which includes the collection optics, spectrograph, and ICCD detector, is calibrated based on a NIST-traceable calibration light source from 220 nm to 1050 nm (DH-2000-CAL deuterium tungsten halogen calibration standard, Ocean Optics). The relative response at each wavelength was obtained by comparing the recorded spectrum of the ICCD with the spectrum of the light source provided by the manufacturer. Fluorescence spectra for single particles are obtained by subtracting an average of background spectra. The average background spectrum (from 200 shots) is recorded under the same experimental conditions, but without particles present by internally firing the laser at 10 Hz. The background counts of the ICCD are mainly from some elastic scattering leakage, stray light, and the thermal and read-out noise of the ICCD.

2.6. Ultraviolet aerodynamic particle sizer (UVAPS)

The Ultraviolet Aerodynamic Particle Sizer® (UVAPS, Model 3314, TSI) is a commercially available system used for real-time monitoring of bioaerosol size and total fluorescence. To help examine the effects of ozone on bioaerosols, a UVAPS is used to measure the aerodynamic particle size distribution and integrated fluorescence (between 430 and 580 nm) intensity distribution excited by a 355-nm laser. Sampling from the drum was limited to 1 LPM by attaching only the inner, sample-flow inlet to the drum and letting the instrument pull the sheath air (4 LPM) from the surrounding laboratory.

2.7. Preparation of bioaerosol materials

Thrombospondin-1 octapeptide powder (American Peptide Co.) was suspended into a mixture of 1:5 PBS to water at a concentration of 0.25 mg/mL. The suspension was divided into 4 mL aliquots and frozen for storage to prevent damage to the peptides. Aliquots were defrosted in the refrigerator prior to aerosolization each day. These suspensions were loaded into syringes with magnetic stir bars for aerosolization with the ultrasonic nozzle.

Bacillus thuringiensis Kurstaki was obtained from Dugway Proving Grounds and resuspended in water at 10 mg/mL for aerosolization. *B. subtilis* was obtained from the U.S. Army Edgewood Chemical Biological Center (ECBC) and suspended in water at 0.025 mg/mL to produce the nominal 1.5 μm size in diameter particles by IJAG for system testing.

2.8. Measurement protocol

Each measurement period lasted for 4 h, with additional time required for ozone conditioning if necessary. Prior to the test, the drum was pre-conditioned to a RH about 5% below the desired humidity to allow for additional moisture that was introduced into the drum by the aerosol generation process. Aerosol was generated and introduced into the chamber for 10 min to reach a particle concentration of approximately 300 particles/cm^3. Once the aerosol reached the desired concentration, initial measurements were made with the UVAPS and SPFS. During these measurements, the airflow out of the drum was balanced by dry air introduced into the drum. If the test required ozone conditioning, ozone was added to the drum for approximately 20 min after the initial

measurements, until the ozone reached a concentration of 150 ppb. The 4-h measurement period then began, with UVAPS and SPFS measurements made every hour. The UVAPS was sampled for 3 min every hour. Its pump was turned off during the rest of the test. During the 3-min sample period, a controller and software activated the ozone and RH control/generation systems, if necessary, to maintain the ozone and RH at their set points. Additionally, the ozone control system was turned on for 2 min every 10 min to maintain ozone levels at approximately 150 ppb during trials at high ozone concentration. Air lost to the UVAPS, SPFS, and ozone monitor was balanced with dry, filtered air sent into the drum. When measurements were not occurring, no air was introduced into or removed from the drum. After the 4-h measurement period, the drum was purged at 55 LPM for about 30 mins, until the aerosol concentration was far below 1% of its starting value.

3. Results and discussion

The new chamber was initially characterized using *Bacillus thuringiensis* Kurstaki particles. Aerosol was generated and injected into the chamber (which rotated at 1 rpm) and measured hourly with a UV-APS over a 9 h period. The measured size distributions were binned according to their fluorescence properties. It is presumed that only the fluorescent fraction of the particles contain spores. During these experiments, the RH was maintained at 30.9% ± 2.8%, temperature was 20.6 ± 0.4 °C, and no ozone was generated. During the 9-h experiment, little change was observed in the particle size distribution (Fig. 2(a) and (b)), although it is apparent that some loss was occurring in the larger, fluorescent particles, particularly after the first 3 h. The number concentration decreased steadily over the 9 h period, in response to both sampling loss during the measurements and settling loss, although even after 9 h ~33% of the initial concentration remained in the chamber.

During a separate experiment, the ability to maintain both a stable RH and ozone concentration simultaneously was observed. Over this 4-h experiment, the target ozone concentration was 150 ppb (the highest used in this study) and the target RH was 50%. After the initial target concentrations were reached, the RH was measured approximately every 10 s (using the internal sensor shown in Fig. 1) and the ozone was measured every 15 min (using an external sensor). We found that the ozone was able to be maintained at 145.4 ppb ± 6.6 ppb. The RH was held at 49.0% ± 2.8%, while the temperature remained constant at 20.4 ± 0.6 °C.

Although the UVAPS was used to measure the size distribution and concentration at any measurement time for the bioaerosol particles within the chamber, it did not accurately reflect the particles sampled by SPFS, which has a different aerodynamic design and only responds to particles larger than 1 μm. In particular, previously described versions of the SPFS cannot supply the individual particle size associated with a measured UV-LIF spectrum. Therefore, a capability to measure the forward elastic scattering from the particles and to estimate the particle size from this scattering was added to the SPFS system. Fig. 3(a) shows the aerodynamic paricle size distribution measured by TSI-APS 3200 and Fig. 3(b) shows the corresponding elastic scattering intensity distribution measured by SPFS for PSL spheres and tryptophan particles with nominal sizes 1 μm, 1.1 μm, 2 μm, 2.3 μm, 3 μm, 3.1 μm, 4.2 μm, and 5.8 μm. The light scattering particle size histograms show reasonable agreement with the aerodynamic size histograms, but exhibit larger uncertainty. The PSL spheres (Duke Scientific) are specified by the manufacturer to have a standard deviation in size of less than 5%. The tryptophan particles produced by the IJAG had a standard deviation greater than 10%. Fig. 3(c) summarizes the average scattering response of the SPFS to 1000 of the PSL and tryptophan particles in multiple tests. A quadratic fit was applied to the scattering intensity versus particle size. The best least squares fit to the data was found to be $I=0.10012-0.04254d+0.28517d^2$, where I is the scattering intensity from the PMT and d is the particle diameter in μm. Using this relation, a particle size can be estimated from its scattering intensity. However, larger errors are expected if the particle has a high absorption at 705 nm, nonspherical shape, different refractive index, or inhomogeneities. For the octapeptide particles studied here, we do not expect large errors from any of these factors because peptide and water have very little absorption at 705 nm, the oxidation products of tryptophan (e.g., kynurenine) have not been reported to absorb strongly at 705 nm, and the dried peptide particles are likely to be approximately spherical with an approximately homogenous refractive index.

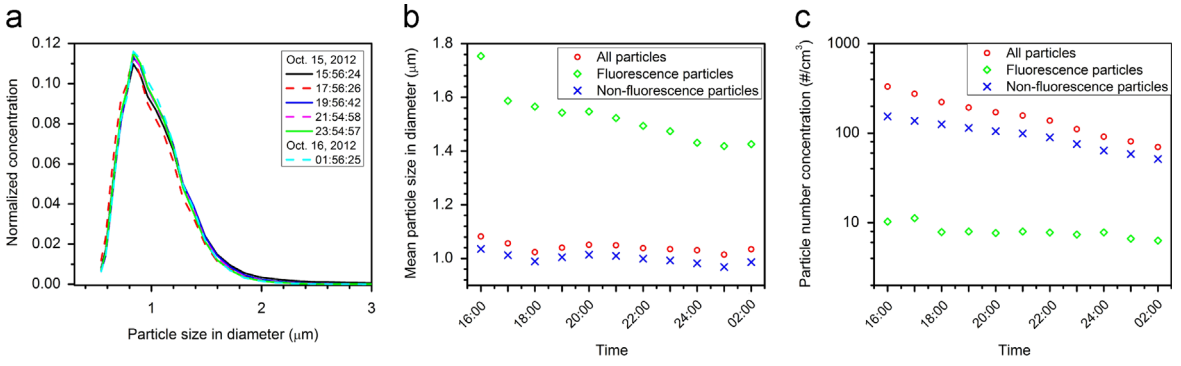

Fig. 2. (a) Particle size distribution, (b) mean particle size, and (c) particle number concentration of the *Bacillus thuringiensis* Kurstaki particles changing over a 9 h period in the rotating chamber.

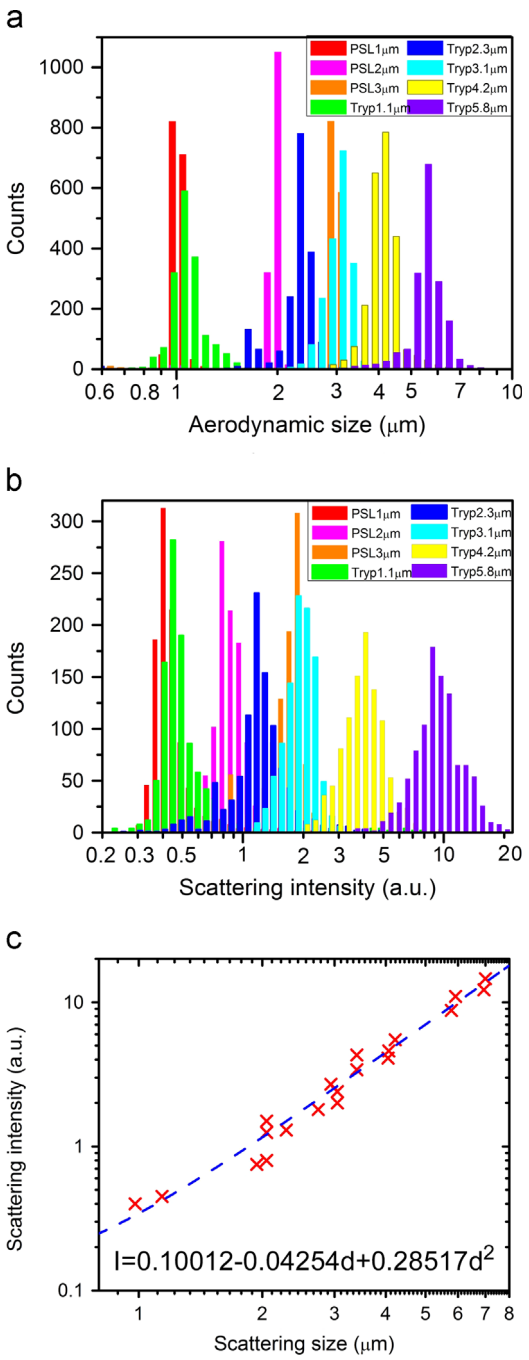

Fig. 3. Histograms of (a) aerodynamic paricle size distribution measured by TSI-APS 3200 and (b) the corresponding elastic scattering intensity distribution measured by SPFS for polystrene (PSL) sphere and tryptophan particles with nominal sizes 1 μm, 1.1 μm, 2 μm, 2.3 μm, 3 μm, 3.1 μm, 4.2 μm, and 5.8 μm. (c) Averaged scattering response of SPFS to the above PSL and tryptophan particles used for calibration. The blue line is a quadratic fit to the data. (For interpretation of the references to color in this figure legend, the reader is referred to the web version of this article.)

Fig. 4 shows 22 successive UV-LIF spectra from single *Bacillus subtilis* particles with a nominated size around 1.5 μm in diameter excited by (a) 263 nm and (b) 351 nm

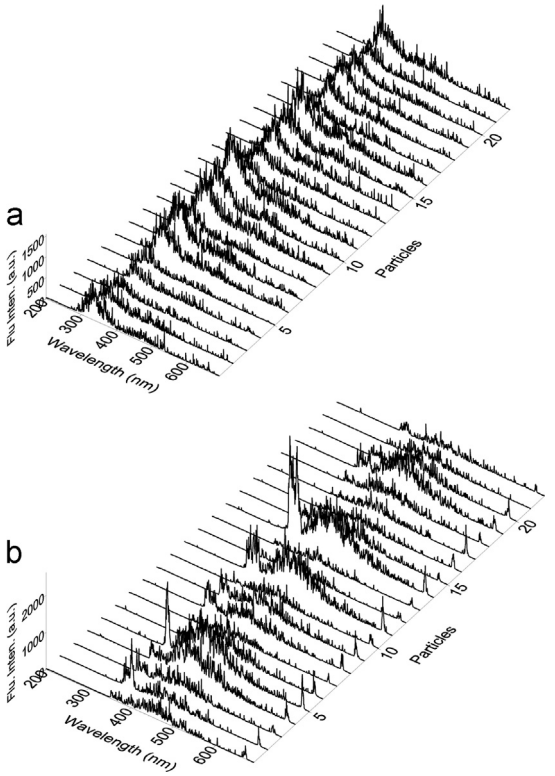

Fig. 4. Successive UV-LIF spectra from 22 single aerosolized *Bacillus subtilis* particles (around 1.5 μm in diameter) excited by (a) 263 nm and (b) 351 nm lasers.

lasers. Each spectrum is generated from a single particle excited by a single pulse of the laser. The sharp peaks around 351 nm and 685 nm (Fig. 4(b)) are the elastic scattering leakage from the UV illuminating laser and one diode trigger laser. The spectra show consistent spectral profiles and good signal to noise (S/N) ratio from particle to particle. The variation in fluorescence intensity from particle to particle depends on several factors, but is dominated by the variation in particle size, which is proportional to the diameter (d) raised to a power typically between 1.8 and 3 [10,35]. Thus for particles in the 1–3-μm diameter range, the range of expected fluorescence is somewhere between 1 to 7.2 and 1 to 27. Other contributions to the particle-to-particle variation for fluorescence intensity are from the changes of (a) total laser fluence ($<5\%$ variation from pulse to pulse), (b) spatial profile of the laser beam, and (c) position of the particle relative to the focal region of the collection optics. Variations in particle composition and the orientation of the particle (particles are not exactly spherical) relative to the illumination and collection optics also contribute to the variations in fluorescence.

Most of the aerosol particles in this study were in the 1–4 μm diameter range with an initial number mean diameter between 2.2 and 2.8 μm (examples are in Fig. 5 (a, d and g)). Typically this mean diameter gradually decreased to around 1.4–2.0 μm by the end of the experiment period (depending on the RH, ozone concentration and total time of the experiment, 4 or 4.5 h). The mean

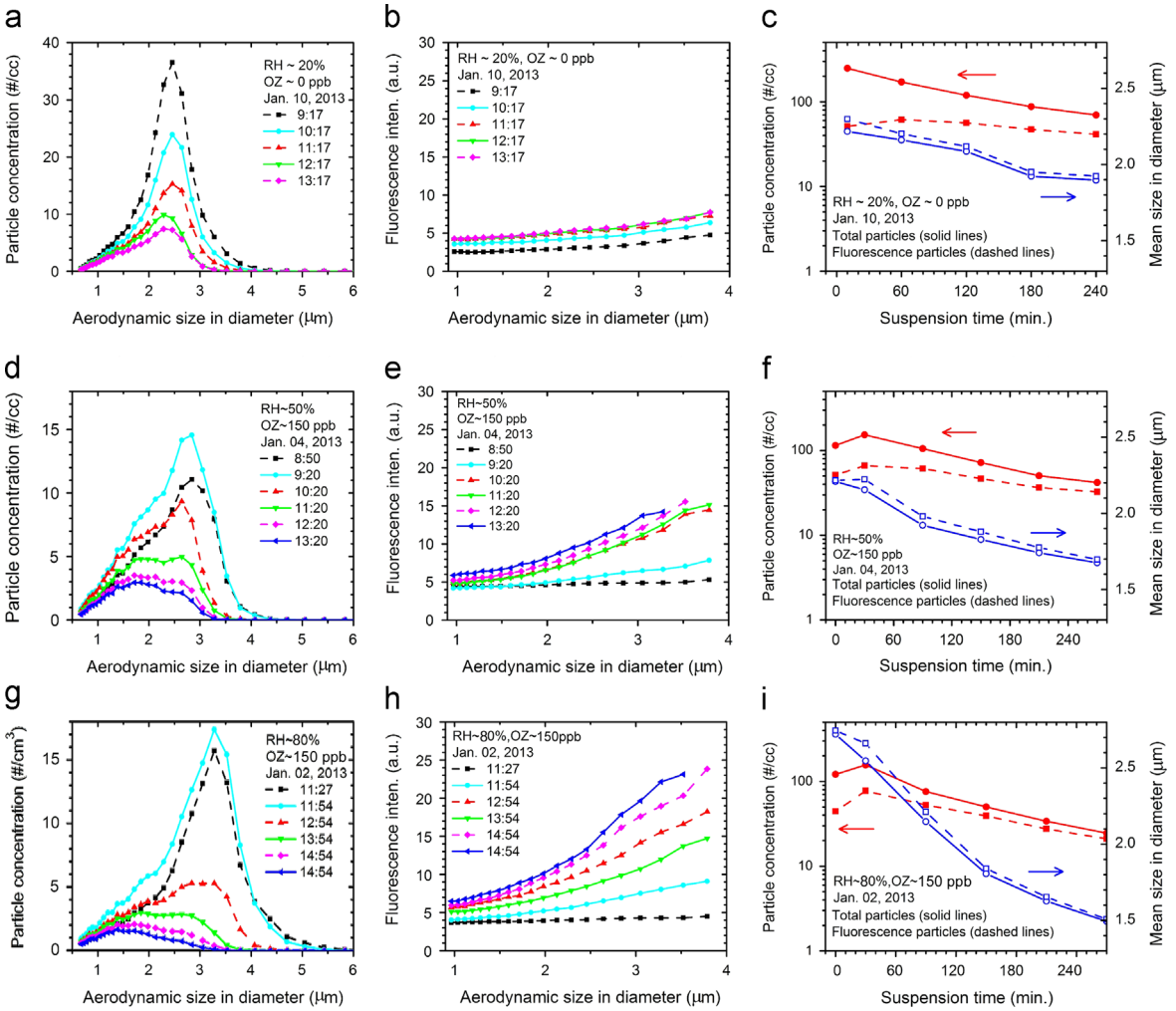

Fig. 5. UVAPS measurements of particle concentrations and fluorescence for different aerodynamic diameters and at various times after octapeptide particles were injected into the rotating drum at the RH and ozone concentrations (OZ) indicated: (a, d and g) are typical total-particle size distributions; (b, e and h) show average fluorescence of particles having fluorescence above a threshold (set at 3 au) for each size bin, plotted vs aerodynamic diameter; (c, f and i) show time-dependent concentrations and mean sizes for total particles and fluorescent particles (For interpretation of the references to color in this figure , the reader is referred to the web version of this article.).

size decreases because of collisions of particles with the drum surface or other surfaces in the chamber, often because of settling. The curves in Fig. 5 show how the concentration and mean size of all the particles and of the fluorescent particles decrease with time, and how they decrease more rapidly when the RH and ozone concentration are larger (Fig. 5f and i). After particles were suspended for 4 or 4.5 h in the chamber the number-mean diameter of all the particles decreased approximately 15%, 25%, and 45% (from the original mean diameter) while the total particle concentration decreased to about 35%, 30%, and 20% (of the peak concentration) for RH and ozone concentrations of 20% and 0 ppb, 50% and 150 ppb, and 80% and 150 ppb, respectively (e.g., Fig. 5c, f and i). The time-dependent changes seen Fig. 5 illustrate that the particle mode size (Fig. 5a, d and g), mean size (Fig. 5c, f and i), and concentration (Fig. 5c, f and i), decrease with time, and that the decrease depends on the RH but has little relationship with ozone concentration. Other measurements (not shown) are consistent with these conclusions. The mean size of fluorescent octapeptide particles (355-nm excitation) decreases at approximately the same rate as the total particles (Fig. 5c, f and i, dashed blue lines). The concentrations of the fluorescent particles, however, decrease more slowly (red dashed lines in Fig. 5c, f and i). The apparent shift in the size distribution and the decrease in concentration are likely caused by the preferential loss of larger particles in the rotating drum, rather than by a change in particle size due to aging. The large loss in concentration over the first 2 h is characteristic of the mixing and initial loss of aerosol in a rotating drum chamber. Over the next 2 h, the concentration dropped more slowly, as is consistent with the decrease being caused primarily by settling and sampling losses. The more rapid decrease in the concentration of large particles at high RH might be due to the adsorption of water vapor which could increase particle mass and make their rate of settling faster than is ideal for the drum and rotation rate used. Adsorption

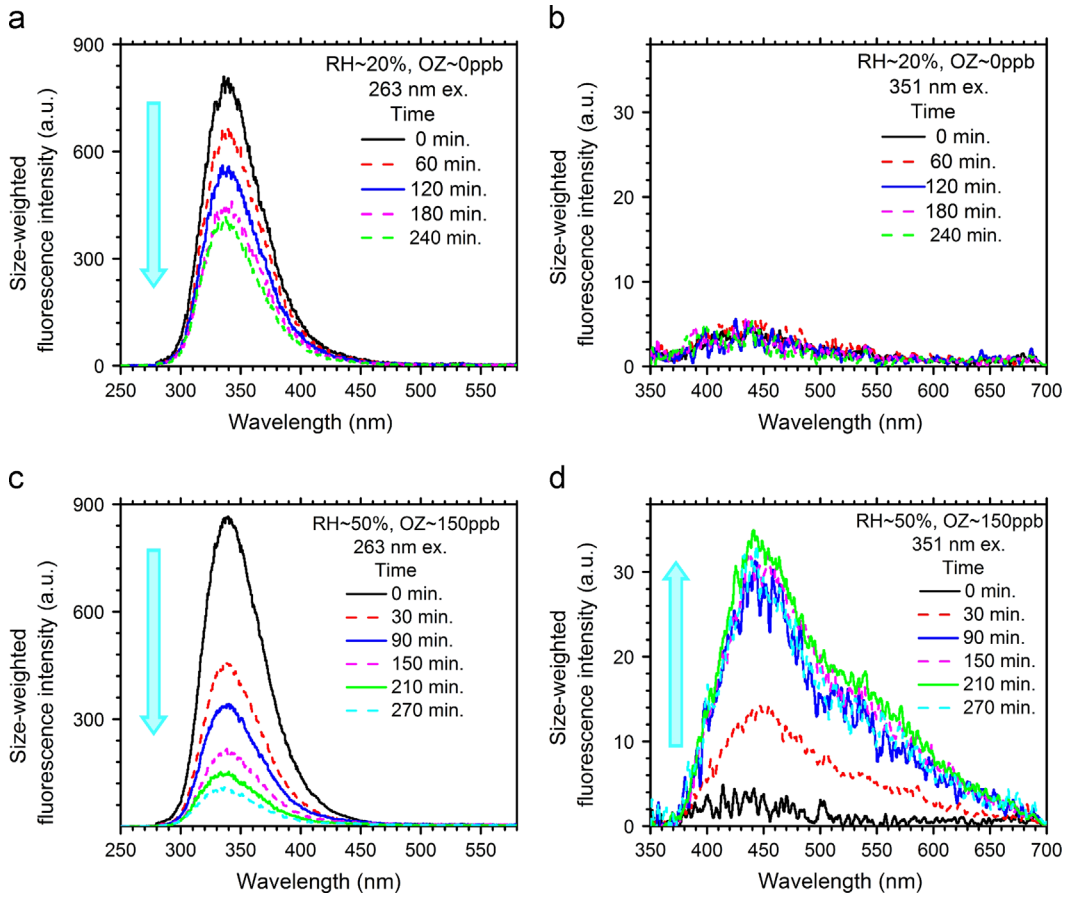

Fig. 6. Typical time-dependent UV-LIF spectra of octapeptide aerosol particles under different RH and ozone concentrations (OZ). In the cases listed at 150 ppb, the ozone increased from approximately 0–150 ppb in the first approximately 30 min. The spectra have been weighted by particle diameter as $1/d^{2.05}$ for 263-nm excitation and as $1/d^{2.8}$ for 351-nm excitation, and so the averaged spectra shown are the converted counts from the measurements of the ICCD that is estimated to be if all particles were 1 μm diameter.

of water could also increase the stickiness of the particles which could lead to more rapid losses to the chamber surfaces.

The integrated fluorescence per particle in each particle size bin (measured by the UVAPS) increased with time at a high ozone concentration and especially at high RH (Fig. 5, middle column). This increase is consistent with Refs. [21–28,30]. When the ozone concentration is low (less than 5 ppb) as seen in Fig. 5b, the increase in 355-nm excited fluorescence is much slower. It suggests that even low ozone concentrations can convert tryptophan to NFK and KN. In Fig. 5(b, e and h) it may appear that the average fluorescence of particles decreases very slowly as the particle size decreases from approximately 2 to 0.9 μm, as if it had reached an asymptote at approximately 3. This behavior should not be taken to suggest that the fluorescence per particle does not decrease as the particles size decreases below 2 μm. The curve appears to reach an asymptote at 3 because a threshold of 3 was used to categorize particles as fluorescent or nonfluorescent. The dynamic range of UVAPS is $2^6=64$, as compared to $2^{16}=65536$ for ICCD.

Fig. 6 shows the averaged UV-LIF spectra excited at 263-nm (left column) and 351-nm (right column). The data in the upper row is for 20% RH and 0 ppb ozone, and in the lower row is for 50% RH and 150 ppb ozone. For each of the four panels three sets of 200 individual aerosolized octapeptide particle were averaged from the measurements at the RH, ozone concentration and exposure times indicated for the various curves. In previous efforts [10,35] it has been noticed that for bioparticles larger than 1 or 2 μm diameter (d) the fluorescence per particle varies approximately as d^x where x is some number that is typically between 1.8 and 3. In averaging the fluorescence we weighted the fluorescence by $1/d^{2.05}$ at 263-nm excitation and by $1/d^{2.8}$ at 355-nm excitation by theoretical estimation. The value of 2.8 at 351 nm is similar to the 2.7 and 2.8 measured for ovalbumin excited at 355 nm [10]. The value of 2.05 at 263 excitation is lower than the three values (2.7, 2.4, and 2.4) reported in Ref. [10] for ovalbumin. However, the mass fraction of 263-nm absorbing amino acids in the octapeptide is larger than it is in ovalbumin, i.e., 11.6 times for tryptophan and 3.85 times for tyrosine, and so the exponent should be smaller than it is for ovalbumin. There are still large uncertainties in the appropriate values for these exponents as can be seen in the measurements of such numbers for albumin [10]. There are also uncertainties in

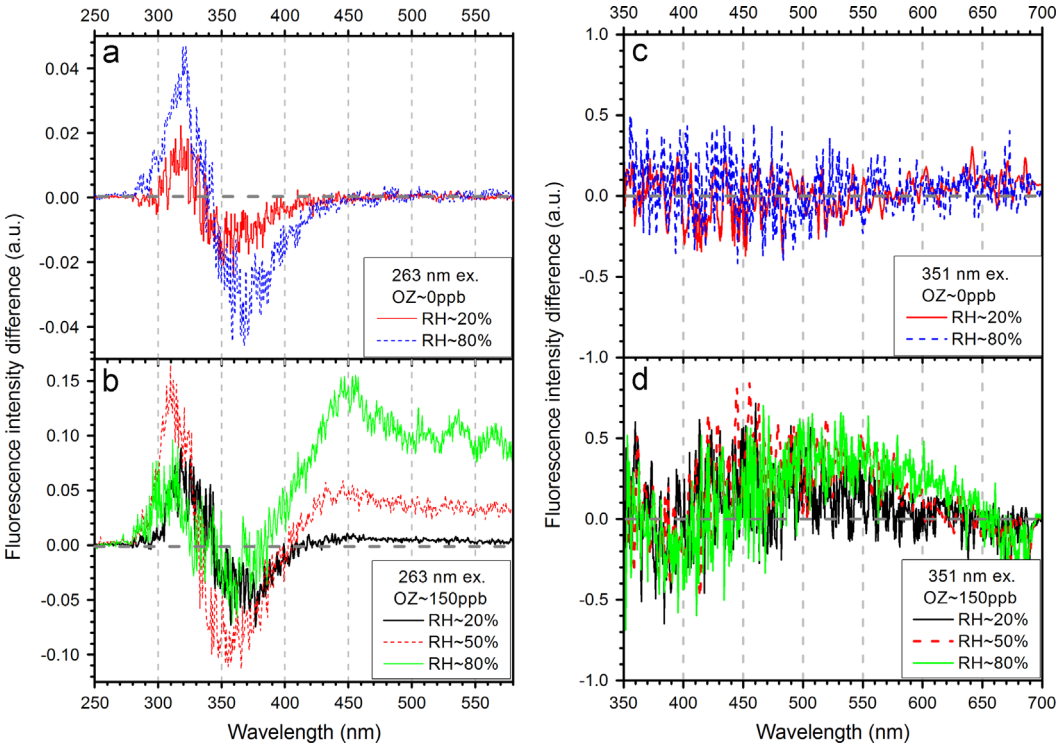

Fig. 7. Fluorescence difference spectra, where each spectrum is the difference between the normalized average fluorescence spectrum at the end of the experiment and the normalized average spectrum when the octapeptide particles were initially released in the chamber. The end of the experiment is after 4 h in the chamber (upper panels with non ozone) or 4.5 h (lower panels with 150 ppb ozone (OZ)) in the chamber. Each curve is an average of three 200-particle sets of spectra. The vertical axis if multipled by 100 gives the percentage change.

trying to model the exponent for 351-nm excited pure proteins or peptides because the absorption by these materials at 355 nm should be almost zero.

In the octapeptide (Arg–Phe–Tyr–Val–Val–Met–Trp–Lys) aerosol particles studied here, Phe, Tyr and Trp absorb strongly at 263 nm. Typically the UV fluorescence of Phe, Tyr and Trp is centered near 280 nm, 300 nm, and 340 nm, respectively, depending upon the local environment. In peptides containing Phe, Tyr and Trp, a significant fraction of the energy absorbed by Phe and Tyr is typically transferred nonradiatively to Trp. The net effect is that the fluorescence from Trp is significantly enhanced, while that of Phe and Tyr is typically negligible or small. Phe, Tyr and Trp have very low absorption coefficients for light at 351 or 355 nm, and other amino acids typically contribute no or negligible absorption or fluorescence for either 263 nm or 351 nm excitation. In Fig. 6, the strong 263-nm-excited fluorescence band centered near 340-nm (left panels) is mainly from tryptophan, with possibly a small contribution from tyrosine and no significant contribution from phenylalanine. This 340-nm band decreased to about one-half of its initial value after 4 h at RH ~20% and ozone <5 ppb (Fig. 6, top left), but decreased faster (reduced by approximately 90%) after 4.5 h at higher RH (50%) and ozone (150 ppb) (lower left). This decrease in the 340-nm band fluorescence is consistent with previous reports of tryptophan reacting with ozone to form ozonides which in the presence of water can be converted to NFK and KN.

Initially, the 351-nm excited fluorescence (Fig. 6, right panels) has a peak intensity about 500 times weaker than does the 263-nm excited fluorescence. This 351-nm excited fluorescence changes little at 20% RH and <5 ppb ozone concentration for 4 h. However, at 50% RH and 150 ppb ozone this fluorescence increased to 20 fold larger than its initial intensity (lower right panel). This increase occurs primarily within the first 1.5 h. Given the composition of the peptide and what is already known about reactions of ozone with tryptophan, this increase in 351-nm excited fluorescence indicates that in these octapeptide particles the ozone caused the oxidation of tryptophan to NFK and/or KN, molecules that fluoresce in the visible when excited at 351-nm (Fig. 6) or 355-nm (Fig. 5). UV-LIF spectra measured at conditions show similar phenomena (see more in Fig. 7).

In order to separate the UV-LIF spectral profile changes from the changes in intensity, all spectra were normalized to one at the peak, and then the initial spectrum, which was measured when the particles were initially released into the chamber, was subtracted to produce the difference spectra. Fig. 7 presents the difference spectral profiles measured initially and after 4 h (with no ozone) or 4.5 h (when ozone is added) of aging in the chamber. All 263-nm excited spectra, with or without ozone, exhibit slight blue shifts in the 340-nm band for an increase in intensity at shorter wavelengths and a decrease at longer wavelengths. These changes in intensity are less than 5% when particles were not exposed to ozone (Fig. 7(a)) but

up to about 10–15% when particles were exposed to ozone at various RH (Fig. 7(b)).

These changes in the spectra profiles may have multiple causes. We speculate that the blue-shift at very low (<5 ppb) (Fig. 7(a)) or high (150 ppb) (Fig. 7(b)) ozone concentration might have contributions from one or more of the following: (1) The ozone (even at less than <5 ppb) may be sufficient to oxidize a significant fraction of the tryptophan while causing less or no decrease in the fluorescence from tyrosine, which has its peak emission near 303 nm, and some emission even at 360 nm. Also, most of the energy absorbed by tyrosine is transferred nonradiatively to tryptophan in typical proteins. As tryptophan is oxidized the transfer of energy from tyrosine to tryptophan should decrease and tyrosine fluorescence should therefore increase. This preferential oxidation of tryptophan is consistent with the order of oxidization rates (Met > Trp > Tyr–His > Phe) observed when ozone was bubbled through water containing *E. coli* or bovine serum albumin [27]. (2) Rearrangements in the secondary, tertiary and quaternary structure of the octapeptide–NaCl–water droplets might occur to allow the aromatic amino acids from different peptides to be more in contact with each other, and to be in a more apolar environment. The fluorescence of tryptophan is known to shift to shorter wavelengths when it moves into a less polar environment [36]. (3) If the room light contains UV-A and pass into the chamber through the end windows of the drum, this UV light could cause the photo-oxidation of tryptophan (to NFK, KN, hydroxykynurenine and several other molecules that are less fluorescent if sufficient water is present [37]). NFK and KN are fluorescent, but possibly the photooxidation occurs in such a manner that some of the products are nonfluorescent molecules by 263 or 351 nm excitation when no ozone is involved.

The relative increase in intensity in the visible wavelength range (400–600 nm) during the exposure to 150 ppb ozone (Fig. 7(b)) indicates that one or more new fluorescent molecules have been generated (as was shown in Fig. 6 for 351-nm excitation), and that this oxidation product can also be excited at 263 nm to fluoresce at visible wavelengths. Because the composition of the octapeptide and the reactions of ozone with tryptophan are known, the primary new molecules that may be responsible for the new fluorescence are NFK, KN and possibly further-modified variants of these such as hydroxykynurenine. Because we do not know how rapidly the NFK would hydrolyze to KN and then to hydroxykynurenine at different RH in these peptide-salt particles we cannot very well estimate the fractions of these metabolites in these particles at different RH at the present study.

At ozone concentrations of <5 ppb there is a negligible increase in visible fluorescence, at 20% or 80% RH, and so it does not appear that NFK and KN are being produced or that tryptophan is being oxidized by ozone. That suggests that the blue shift seen at <5 ppb ozone is not caused by the oxidation of tryptophan but by a rearrangement of the peptide to a less polar environment, or by photo-oxidation of tryptophan to produce non-fluorescent molecules, but we have no indication that there is sufficient light to cause that.

Fig. 8 summarizes the time-dependent UV-LIF band intensity and intensity ratio changes under different experimental conditions (combinations of RH around 20%, 50%, or 80% and ozone concentration about 0 or 150 ppb). All data points were averaged from 3 data sets, which were measured on different days with the same experimental conditions, and each data set contains 200 UV-LIF spectra from 200 single aerosolized octapeptide particles around the same elapsed time in the chamber after initial release. The fluorescence intensities from all spectra were also converted into ICCD count/per 1 μm diameter equivalent particle (as in Fig. 6) to eliminate the size decay effect. UV263 is the integrated fluorescence band intensity from 280 nm to 400 nm excited at 263-nm; Vis263 is the band intensity from 400 nm to 580 nm excited at 263-nm; and Vis351 is the band intensity from 380 nm to 700 nm excited at 351-nm. The three fluorescence band intensities decrease slowly (a), with similar decay rate (b) at low RH (20%) and ozone concentration ($\sim$0 ppb), and with a slightly faster decrease for the UV band at high RH (80%) with the absence of ozone (c and d).

Once the ozone is added to the chamber (150 ppb), the 263-nm excited UV fluoresecnce band decreases more rapidly for increasingly higher RH (from 20%, to 50%, then 80%), but the rate of change of the 263-nm excited visible fluorescnce band, composed of emissions from both the tryptophan tail and the products of tryptophan oxidation, does not appear to change significantly. When ozone is present, the magnitude of the 351-nm excited visible fluoresecnce band increases more rapidly at higher RH, particularly at the begining, and then slows down once it reaches a certain intensity level (Fig. 8(e, g and i)). This band is produced mainly from the products of the ozone reaction that can be strongly excited by a 351-nm laser, and only a little from tryptophan. The intensity ratio changes (Fig. 8(f, h and j)) indicate that the 263-nm excited UV fluorescence band always decreases faster than the visible band (red lines), and the visible fluorescence band excited by 351-nm excitation always increases faster than the 263-nm excitation, and such changes happen increasingly quickly with the increase of RH in the presence of ozone.

For aerosolization, the octapeptide was suspended in PBS, i.e., phosphate buffered saline. The NaCl in the particle is probably much more hygroscopic than the peptide, which has three aromatic amino acids out of eight, and three more non-polar amino acids. Little liquid water is likely to remain on these particles even at 20% RH, and the particles at low RH should contain less water than particles of the same size at high RH. Increased RH appears to increase the reaction rates of the particles with ozone and the visible fluorescence intensities increase more rapidly. The deduced or size-weighted fluorescence intensity comparison would be more accurate if we were able to measure the water fraction of the particle and take it into account.

Aqueous tryptophan can be converted by ozone to NFK and KN [21–28]. UV light, including UV-A, can photodegrade proteins [37–40], generating several fluorescent products of tryptophan, including NFK, KN and hydroxykynurenine [37], and several products of tyrosine. KN has a

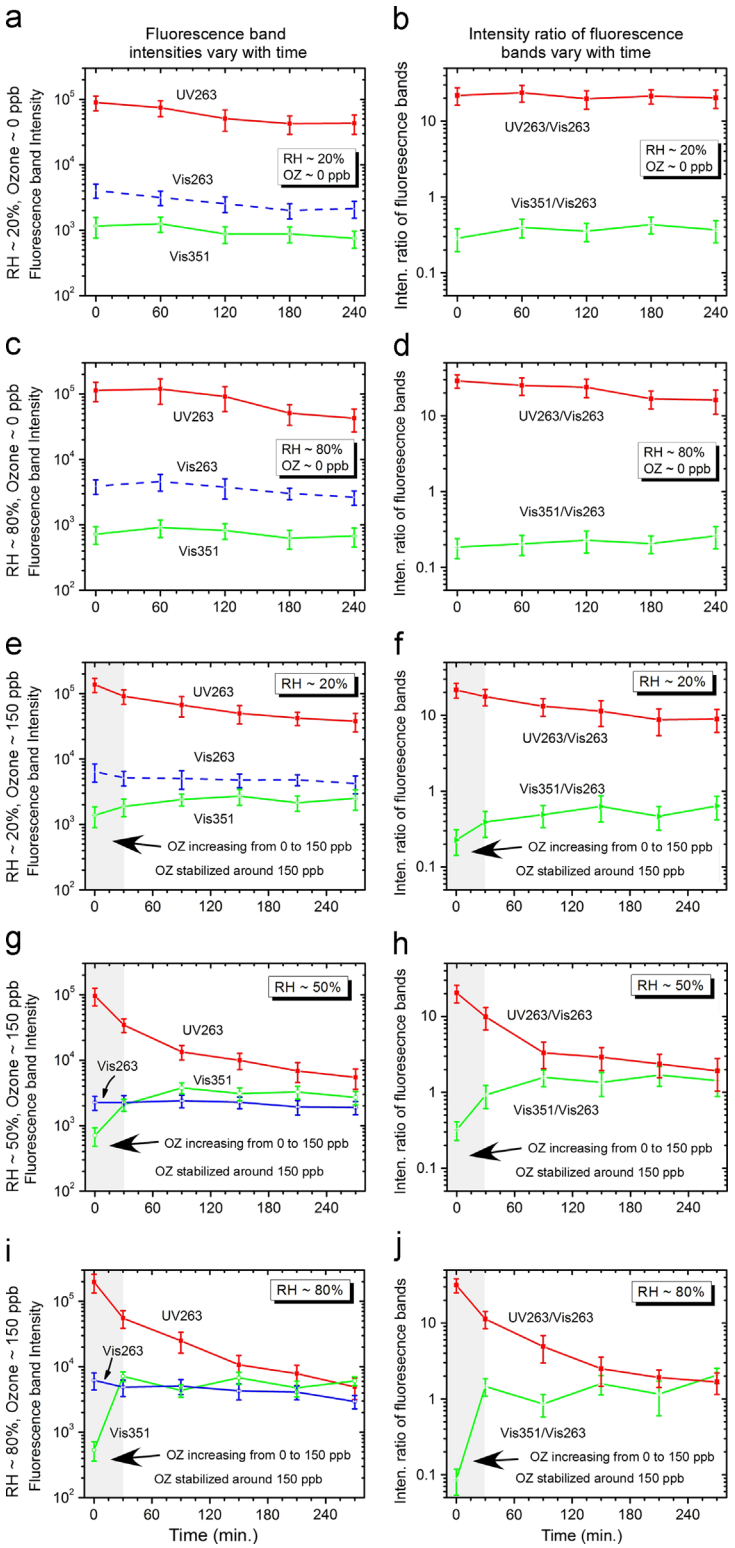

Fig. 8. Averaged intensities and intensity ratios of UV-LIF bands from octapeptide aerosol particles vs time with different experimental conditions (combinations of RH at 20%, 50%, or 80% and ozone (OZ) at 0 or 150 ppb). In all cases the ozone is <5 ppb for the measurement at time=0 min. In the panels marked 150 ppb, the ozone gradually rose from <5 ppb to 150 ppb within the first 30 min (left gray area). UV263 is the integrated fluorescence band intensity from 280 nm to 400 nm excited by 263-nm lasetr. Vis263 is the fluorescence from 400 nm to 580 nm excited by 263 nm laser. Vis351 is the band from 380 nm to 700 nm excited by 351-nm laser. The spectra have been weighted by particle diameter as $d^{2.05}$ for 263-nm excitation and as $d^{2.8}$ for 351-nm excitation, and so the averaged spectra shown are the counts on the ICCD that would would be measured if all particles were 1 μm diameter (For interpretation of the references to color in this figure, the reader is referred to the web version of this article.).

wide fluorescence emission band in the visible, peaking around 430–490 nm, and has absorption peaks near 360 nm and 260 nm. The fluorescence is much stronger when KN is covalently attached to amino acids. NFK fluoresces in a similar wavelength region and has a strong absorption peak around 330 nm and a small absorption peak at 265 nm [e.g., 39,40]. For the octapeptide with the sequence Arg–Phe–Tyr–Val–Val–Met–Trp–Lys studied here, only phenylalanine, tyrosine, and tryptophan emit UV fluorescence when excited at 263-nm and fluoresce very little when excited at 351-nm. By checking the possible oxidization products or modification of molecules by various oxidizing sources [e.g., 41], NFK and KN (from tryptophan) and dityrosine (from tyrosine) are the main fluorescent molecules that can be produced by interaction with ozone. Dityrosine has high absorption around 315 nm and also absorbs strongly at 263 nm but absorbs very little at wavelengths above 350 nm. It fluoresces around 350–500 nm with a peak at 408 nm when excited at 325-nm [42]. In the fluorescence spectral profile excited at 351-nm (Fig. 6(d)) and the spectral profile changes by 263-nm and 351-nm excitation (Fig. 7), it appears that the new products fluoresces in the visible wavelength range (400–700 nm) and is peaked around 450 nm when excited at 351-nm or 263-nm. These measurements are consistent with previous studies of pure amino acids in aqueous suspensions, where KN was produced when tryptophan interacted with ozone [21–23,25–28], where the observed fluorescence emission is primarily from the oxidation product KN, with possible small contributions from dityrosine and NFK. However, in the aerosolized peptide-salt particles studied here, the water activity is much lower than in typical aqueous media, especially at the lower humidities (RH=20% or 50%) and so the conversion of NFK to KN will be less rapid than it is in aqueous solutions. Previous studies have also observed that a more rapid uptake of ozone by amorphous protein particles happens at higher humidity [43–44]. Our measurements also show that the oxidation is more rapid at higher RH.

The typical ambient ozone concentrations found in remote continental measurements are from 1 to 125 ppb dependent on altitude, atmospheric conditions and local conditions. The typical peak concentrations in American cities are between 150 and 510 ppb [45]. Therefore, the changes in florescence spectral intensities and profiles of biological particles observed in the laboratory simulated conditions here (RH around 20%, 50%, or 80% and ozone around 0 or 150 ppb) are potentially important in the atmosphere. These changes in fluorescence may significantly impact fluorescence-based detection of biological aerosols that were exposed to atmospheric ozone under similar conditions.

4. Summary

A laboratory system, improved over our previous apparatus [30], for studying the changes in bioaerosol particles in simulated atmospheric environments was developed. Aerosolized octapeptide (Arg–Phe–Tyr–Val–Val–Met–Trp–Lys) particles (mostly in the 1–4 μm diameter size range with a mean size around 2 μm) were injected into a rotating reaction chamber and suspended inside for 4 or 4.5 h of observation under controlled RH (20%, 50%, or 80%) and ozone concentration (0 or 150 ppb). Hourly measurements of the octapeptide bioaerosol particles sampled from the chamber show the following: (1) Particle size, concentration, and the 263-nm-excited fluorescence intensity decrease at different rates under different combinations of the RH and ozone concentrations used. (2) The 263-nm-excited UV fluorescence (280–400 nm) decreases with time, which is consistent with the oxidation of tryptophan molecules. (3) The UV fluorescence peak near 340 nm slightly shifts to shorter wavelengths with time elapse, possibly because tryptophan oxidizes faster than tyrosine does. (4) The 351- and 355-nm-excited fluorescence increases when ozone is present, especially when the RH is high. (5) The increase in fluorescence emission in the visible that occurs with the decrease of tryptophan emission is due primarily to increases in NFK and KN, which have been reported to be two of the main products of ozonolysis–hydrolysis of tryptophan. This study provides a better understanding of the changes in bioaerosols and their properties occurring in the atmospheric environment, and suggests limitations of fluorescence-based bioaerosol measurements, particularly in environments where moderate to high ozone concentrations may exist.

Acknowledgments

This research was supported by the Defense Threat Reduction Agency (DTRA) under contract number HDTRA1-10-C-0023, and by US Army Research Laboratory (ARL) mission funds.

References

[1] Despres V, Huffman AJ, Burrows SM, Hoose C, Safatov AS, Buryak G, et al. Primary biological aerosol particles in the atmosphere: a review. Tellus 2012;B 64(15598):1–58.
[2] Fiegel J, Clarke R, Edwards D. Airborne infectious disease and the suppression of exhaled aerosols. Drug Discovery Today 2006;11(1–2):51–7.
[3] Sun JM, Ariya PA. Atmospheric organic and bio-aerosols as cloud condensation nuclei (CCN): a review. Atmos Environ 2006;40(5):795–820.
[4] Pohlker C, Huffman JA, Pöschl U. Autofluorescence of atmospheric bioaerosols–fluorescent biomolecules and potential interferences. Atmos Meas Tech 2012;5:37–71.
[5] Pan YL, Eversole JD, Kaye P, Foot V, Pinnick RG, Hill SC, et al. Bio-aerosol fluorescence. In: Hoekstra A, Maltsev V, Videen G, editors. Optics of biological particles. The Netherlands: Springer; 2006. p. 63–164.
[6] Reyes FL, Jeys TH, Newbury NR, Primmerman CA, Rowe GS, Scanchez A. Bio-aerosol fluorescence sensor. Field Anal Chem Technol 1999;3:240–8.
[7] Kaye PH, Stanley WR, Hirst E, Foot EV, Baxter KL, Barrington S. Single particle multichannel bio-aerosol fluorescence sensor. Opt Express 2005;13:3583–93.
[8] Pan YL, Hartings J, Pinnick RG, Hill SC, Halverson J, Chang RK. Single-particle fluorescence spectrometer for ambient aerosols. Aerosol Sci Technol 2003;37(8):628–39.
[9] Pan YL, Hill SC, Pinnick RG, Huang H, Bottiger JR, Chang RK. Fluorescence spectra of atmospheric aerosol particles measured using one or two excitation wavelengths: comparison of classification schemes employing different emission and scattering results. Opt Express 2010;18(12):12436–57.
[10] Sivaprakasam V, Lin HB, Huston AL, Eversole JD. Spectral characterization of biological particles using two-wavelength excited laser-induced

fluorescence and elastic scattering measurements. Opt Express 2011;19(7):6191–208.
[11] Pan YL, Pinnick RG, Hill SC, Rosen JM, Chang RK. Single-particle laser-induced-fluorescence spectra of biological and other organic-carbon aerosols in the atmosphere: measurements at New Haven, CT and Las Cruces, NM, USA. J Geophys Res 2007;112:D24S19.
[12] Gabey AM, Gallagher MW, Whitehead J, Dorsey J, Kaye PH, Stanley WR. Measurements and comparison of primary biological aerosol above and below a tropical forest canopy using a dual-channel fluorescence aerosol spectrometer. Atmos Chem Phys 2010;10:4453–66.
[13] Pinnick RG, Fernandez E, Rosen JM, Hill SC, Wang Y, Pan YL. Fluorescence spectra and elastic scattering characteristics of atmospheric aerosol in Las Cruces, New Mexico, USA: variability of aoncentrations and possible constituents and sources of particles in various spectral clusters. Atmos Environ 2013;65:195–204.
[14] Dark FA, Nash T. Comparative toxicity of various ozonized olefins to bacteria suspended in air. J Hygiene 1970;68(2):245–52.
[15] Dungan RS. Fate and transport of bioaerosols associated with livestock operations and manures. J Anim Sci 2010;88:3693–706.
[16] Rudich Y, Donahue NM, Mentel TF. Aging of organic aerosol: bridging the gap between laboratory and field studies. Ann Rev Phys Chem 2007;58:321–52.
[17] Bailey R, Fielding L, Young A, Griffith C. Effect of ozone and open air factor against aerosolized *Micrococcus luteus*. J Food Prot 2007;70(12):2769–73.
[18] Kanaania H, Hargreavesa M, Ristovskia Z, Morawskaa L. Performance assessment of UVAPS: influence of fungal spore age and air exposure. J Aerosol Sci 2007;38:83–96.
[19] Roshchina VV, Melnikova EV. Pollen chemosensitivity to ozone and peroxides. Russ J Plant Physiol 2001;48(1):74–83.
[20] Adhikari A, Reponen T, Grinshpun SA, Martuzevicius D, LeMasters G. Correlation of ambient inhalable bioaerosols with particulate matter and ozone: a two-year study. Environ Pollut 2006;140(1):16–28.
[21] Ignatenko AV, Tatarinov BA, Khovratovich NN, Khrapovitskii VP, Cherenkevich SN. Spectral-fluorescent investigation of the action of ozone on aromatic amino acids. J Appl Spectrosc 1982;37(1):781–4.
[22] Ignatenko AV. Use of the method of tryptophan fluorescence to characterize disruptions of the structure of ozonized proteins. J Appl Spectrosc 1988;49(1):691–5.
[23] Fujimori E. Changes induced by ozone and ultraviolet light in type I collagen Bovine Achilles tendon collagen versus rat tail tendon collagen. Eur J Biochem 1985;152(2):299–306.
[24] Nisimoto Y, Shibata Y. Studies on FAD- and FMN-binding domains in NADPH-cytochrome P-450 reductase from rabbit liver microsomes. J Biol Chem 1982;257(21):12532–9.
[25] Mudd JB, Dawson PJ, Tseng S, Liu FP. Reaction of ozone with protein tryptophans: band III, serum albumin, and cytochrome C. Arch Biochem Biophys 1997;388:143–9.
[26] Kotiaho T, Eberlin MN, Vainiotalo P, Kostiainen R. Electrospray mass and tandem mass spectrometry identification of ozone oxidation products of amino acids and small peptides. J Am Soc Mass Spectrom 2000;11:526–35.
[27] Berlett BS, Levine RL, Stadtman ER. Comparison of the effects of ozone on the modification of amino acid residues in glutamine synthetase and bovine serum albumin. J Biol Chem 1996;271(8):4177–82.
[28] Pryor WA, Uppu RM. A kinetic model for the competitive reactions of ozone with amino acid residues in proteins in reverse micelles. J Biol Chem 1993;268(5):3120–6.
[29] Pan YL, Pinnick RG, Hill SC, Niles S, Holler S, Bottiger JR, et al. Dynamics of photon-induced degradation and fluorescence in riboflavin microparticles. Appl Phys B 2001;72:449–54.
[30] Santarpia JL, Pan YL, Hill SC, Baker N, Cottrell B, McKee L, et al. Changes in fluorescence spectra of bioaerosols exposed to ozone in a laboratory reaction chamber to simulate atmospheric aging. Opt Express 2012;20(28):29867–81.
[31] Goldberg LJ, Watkins HMS, Boerke EE, Chatigny MA. The use of a rotating drum for the study of aerosols over extended periods of time. Am J Hygiene 1958;68:85–93.
[32] Gruel RL, Reid CR, Alleman RT. The optimum rate of drum rotation for aerosol aging. J Aerosol Sci 1987;18:17–22.
[33] Ratnesar-Shumate SR, Wagner ML, Kerechanin C, House G, Brinkley KM, Bare C, et al. Improved method for the evaluation of real-time biological aerosol detection technologies. Aerosol Sci Technol 2011;45:635–44.
[34] Santarpia JL, Gasparini R, Li R, Collins DR. Diurnal variations in the hygroscopic growth cycles of ambient aerosol populations. J Geophys Res 2005;110:D03206.
[35] Hill SC, Pinnick RG, Niles S, Fell NF, Pan YL, Bottiger J, et al. Fluorescence from air-borne microparticles: dependence on size, concentration of fluorophores, and illumination intensity. Appl Opt 2001;40:3005–13.
[36] Lakowicz JR. Principles of fluorescence spectroscopy. New York: Plenum; 534–9.
[37] Grosvenor AJ, Morton JD, Dyer JM. Profiling of residue-level photo-oxidative damage in peptides. Amino Acids 2010;39:285–96.
[38] Sherin PS, Grilj J, Kopylova LV, Yanshole VV, Tsentalovich YP, Vauthey E. Photo-physics and photochemistry of the UV filter kynurenine covalently attached to amino acids and to a model protein. J Phys Chem B 2010;114(36):11909–19.
[39] Shacter E. Quantification and significance of protein oxidation in biological samples. Drug Metab Rev 2000;32(3&4):307–26.
[40] Caldwell CR. Ultraviolet-induced photodegradation of cucumber (*Cucumis sativus* L.) microsomal and soluble protein tryptophanyl residues in vitro. Plant Physiol 1993;101(3):947–53.
[41] Sharma VK, Graham NJD. Oxidation of amino acids by ozone: A review. Ozone: Sci and Eng 2010;32(2):81–90.
[42] Mahmoud SF, Bialkowski SE. Laser-excited fluorescence of dityrosine. Appl Spectrosc 1995;49(11):1669–76.
[43] Shiraiwa M, Ammann M, Koop T, Pöschl U. Gas uptake and chemical aging of semisolid organic aerosol particles. Proc Natl Acad Sci USA 2011;108(27):11003–8.
[44] Shiraiwa M, Sosedova Y, Rouvière A, Yang H, Zhang Y, Abbatt JP, et al. The role of long-lived reactive oxygen intermediates in the reaction of ozone with aerosol particles. Nat Chem 2011;3(4):291–5.
[45] ⟨http://www.ozonelab.com/index.htm⟩.